ELSEVIER

Polymer 44 (2003) 89–100

polymer

www.elsevier.com/locate/polymer

Probing the morphology of polypropylene fibres by scanning probe microscopy

Ole K. Risnes[a,b,*], Robert R. Mather[a,1], Anne Neville[b,2]

[a]*School of Textiles, Heriot-Watt University, Netherdale, Galashiels TD1 3HF, UK*
[b]*Corrosion and Surface Engineering Research Group, Heriot-Watt University, Riccarton, Edinburgh EH14 4AS, UK*

Received 23 May 2002; received in revised form 26 September 2002; accepted 10 October 2002

Abstract

This paper highlights the application of scanning probe microscopy, notably atomic force microscopy in contact mode supported by lateral force microscopy, to the investigation of changes in the morphology of polypropylene (PP) monofilaments during melt-extrusion and subsequent drawing. A gradual deformation at the fibre surface from a spherulitic structure to a shish-kebab type structure is observed for the gravity spun and as-spun variants. In the drawn PP filaments, the surface structure is predominantly fibrillar in character, though the nature of the fibrillar structure is influenced by the drawing conditions. Wide angle X-ray scattering analysis, in conjunction with SPM, indicates contrasting features of surface and bulk crystal structure both at the as-spun and drawn stages of production. In addition, an unusual WAXS diffraction pattern is observed for the cold drawn PP filament. Studies of the bulk structures of the fibres by investigating fibre cross-sections using SPM will be the subject of a companion paper.

Keywords: Polypropylene; Atomic force microscopy; Paracrystalline

1. Introduction

Scanning probe microscopy (SPM), particularly in the form of atomic force microscopy (AFM) has now attained relative maturity as a surface analytical tool for the analysis of a range of materials ranging from soft biological tissues to semiconductors [1,2]. A general introduction to SPM technology can be found elsewhere [3].

In fibre science, by contrast, only a few papers making use of SPM technology have been published to date. These have concentrated on wool [4–7], polypropylene [8–11], polyethylene [12,13], carbon [14], Kevlar [15–18] and various composite fibres such as nylon or polypropylene reinforced with carbon or aramid fibres [19–21]. To control production parameters better, in the case of synthetic textile fibres, it is necessary to gain as much information as possible about the microstructure of the fibre at all stages of production and hence accurately define structure/property relationships. In addition to the bulk properties of a textile fibre, its surface properties should also be taken into account, as these also play a fundamental role in governing some key technical properties. Like bulk properties, surface properties are to a large extent related to fibre processing conditions [22].

It has been demonstrated successfully that SPM can provide new information on surface morphology of fibres. One of the first papers utilising AFM on textile fibres was published in 1993 by Li et al. [15]. This work, together with research by Rebouillat et al., proved to be significant in the study of Kevlar fibres as the AFM results made it possible to clarify aspects of existing proposed structural models due to the visualisation of structural features previously inaccessible [16,17]. With new application areas for textiles constantly emerging, in particular within industrial, engineering and medical textiles [23], there is an increasing need to acquire fundamental knowledge on these materials' microstructure since the design of their macroscopical properties ultimately depend on this.

Polypropylene fibres have had a significant success in the technical textiles sector [24]. It is a highly versatile polymer type and during melt spinning production the structure can be customised, depending on the settings of a wide variety of parameters, to meet the needs of different technological applications, as demonstrated by Yang et al. [25]. Work by

* Corresponding author. Address: School of Textiles, Heriot-Watt University, Netherdale, Galashiels TD1 3HF, UK. Tel.: +44-131-449-5111x2215; fax: +44-1896-758965.
E-mail addresses: o.k.risnes@hw.ac.uk (O.K. Risnes), r.r.mather@hw.ac.uk (R.R. Mather), a.neville@hw.ac.uk (A. Neville).
[1] Tel.: +44-131-449-5111; fax: +44-1896-758965.
[2] Tel.: +44-131-449-5111; fax: +44-131-449-5153.

0032-3861/03/$ - see front matter © 2002 Elsevier Science Ltd. All rights reserved.
PII: S0032-3861(02)00747-4

Hautojarvi et al. [9] and De Rovere et al. [11] on PP fibres have contributed to the understanding of surface morphology development. The gradual transformation from a spherulitic morphology to a fibrillar structure as the filaments were stretched was found in both cases. Hautojarvi et al. found the surface structure of as-spun fibres to be spherulitic, whereas De Rovere et al. only found evidence of spherulites in gravity spun filaments and in the case of as-spun fibres observed a 'shish-kebab' structure. Shish-kebab structures have been defined as fibrous crystals overgrown epitaxially by lamellar crystals, the stems of which are parallel to the fibre axis [26]. Hautojarvi et al. also demonstrated how a fibrillar surface structure is initiated through the deformation of spherulites. This transformation was found to be completed by the stretch of lamellar stacks into nanofibrillar chains. Hautojarvi et al. found, through wide angle X-ray scattering (WAXS) analysis of drawn fibres, that the fibre's crystallinity increased significantly if drawn at higher temperatures relative to room temperature, but with no apparent difference in surface morphology when observed by AFM. The explanation for this was that the continued crystallisation with increase in temperature took place mainly in the core.

One of the main challenges in analysing textile fibres with SPM techniques is the fact that the sample presented to the cantilever tip is curved and often fairly corrugated. This limits the range of techniques or modes applicable and the variations in possible scanning parameters. However, as magnification is increased, and the typical $x-y$ scan size is reduced, the relative corrugation and curving become less of a factor and the possibility of using other techniques without producing a range of artefacts becomes feasible. LFM was found to be particularly well suited in conjunction with AFM to reveal surface features when the scan range was between 5 μm × 5 μm and 200 nm × 200 nm. This has also been demonstrated by Nie et al. on PP films [27].

This paper presents the results from SPM characterisation of the surface morphology of PP melt spun fibres as it develops from gravity spun, via as-spun to fully drawn filaments. These are subsequently correlated with WAXS data for the same filaments. The results are compared with, and discussed in relation to, existing literature on SPM analysis of PP fibres, but also in relation to the extensive research published on morphology development for bulk PP materials. The choice of methodology for SPM analysis of fibres to increase the amount of reliable information extractable from such analysis is also discussed, based on the use of contact mode AFM and LFM.

2. Experimental

2.1. PP filaments

2.1.1. Gravity spun and as-spun filaments

The type of PP raw material used was: polypropylene HF445J B2-9037 from Borealis, with a melt flow index (MFI) of 19.0 g/10 min quoted by the manufacturer. Our tested MFI of the PP raw material was found to be 20.5 g/10 min, as determined by a Ceast 100 plastometer at Beckton Dickinson UK Ltd. in accordance with the ASTM D1238 procedure.

The PP monofilament was spun on a Labspin extruder (Extrusion System Limited (ESL), with a 2.5 cm^3 metering pump and a single hole spinneret with a diameter of 0.50 mm. Barrel temperatures were 210, 215, and 225 °C, respectively, for the three barrel zones. Metering pump temperature was 230 °C with a pump speed at 1 rpm^{-1}, corresponding to an extrusion rate of 4.0 m min^{-1}. The die head temperature was 235 °C and the extruded filament was cooled in an air chamber at 23 °C (± 1 °C) with airspeed set to zero to avoid non-uniform cooling [28]. The gravity spun filaments were collected 1.5 m below the die-head in the air-quench chamber. The as-spun filaments were spun on to a winding roller with a winding speed (take-up speed) varying from 100 to 400 m min^{-1}. No spin finish was applied.

2.1.2. Drawn filaments

Post-drawing of the as-spun monofilament produced at a winding speed of 200 m min^{-1} was carried out on a lab-scale apparatus consisting of two pairs of advancing rollers with a u-shaped heated channel in between. For cold drawing (23 °C) the feeding pair of rollers had a speed of 15.0 m min^{-1} with the take-up rollers set to 60.0 m min^{-1}. The same roller speed was used for 1-stage hot drawing at a temperature of 60 °C. For 2-stage hot drawing the filament from 1-stage hot drawing was processed a second time at 150 °C with feeding rollers at 20.0 m min^{-1} and take-up rollers at 50 m min^{-1}. The length of the heated channel was 61.0 cm^{-1}. The distance from channel wall to filament was in the region of 0.3–0.5 cm.

2.1.3. SPM procedures

The SPM used in this work was a Topometrix TMX 2000 Explorer (TM Microscopes). The scanner head had a maximum scan range in x, y, z direction of 100 × 100 × 8 μm, respectively. Scanning was carried out in contact mode AFM and LFM with a silicon nitride cantilever with a nominal spring constant of 0.03 N m^{-1}. The vertical and lateral deflection of the cantilever, which are used, respectively, to obtain topographic (AFM) and lateral force images (LFM), are detected by a quadrant photodetector via a laser light reflected from the back of the cantilever. The measured cantilever deflection in AFM is generated into a surface topography map of the sample. For LFM scanning the twisting or lateral forces experienced by the cantilever are usually caused by variations in surface friction and changes in slope. LFM scanning should be carried out simultaneously with AFM to separate one effect from the other. Constant force was employed by the cantilever during scanning with a set point in the range of 5–35 nA (force is related to the detector current). All

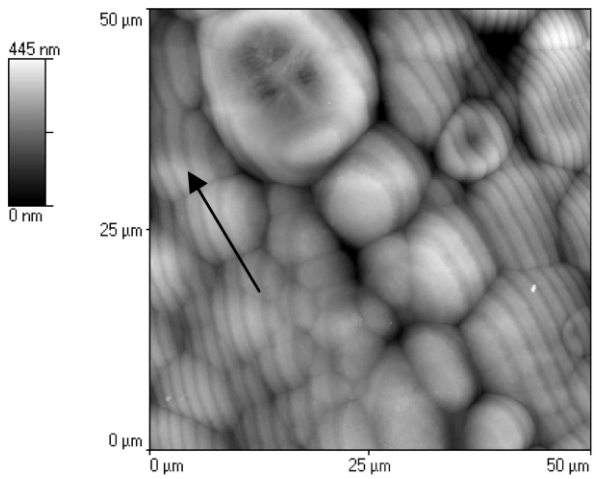

Fig. 1. Topography of gravity spun PP scanned by AFM in contact mode.

images were obtained at ambient conditions. Each fibre sample was mounted to doublesided SEM tape on magnetic AFM sample stubs.

2.1.4. WAXS analysis

WAXS diffraction traces were obtained using a Siemens D500 powder diffractometer (Cu Kα radiation, Ni filtered), equipped with a scintillation counter detector. The scan range was 3–30° (2θ) at a rate of 0.02° s^{-1}. Flat disc samples (diameter 14 mm and thickness 0.5 mm) were made by handpressing tiny lengths of fibres (<1 mm) between glass slides. These were then fitted into a sample holder.

3. Results

3.1. Gravity spun

Fig. 1 shows a 50 × 50 µm AFM topography scan of the gravity spun PP surface. This was the maximum area possible to scan in practice, mainly due to the cantilever *z*-resolution limitations. From the AFM image (Fig. 1) it is clear that the surface is comprised of spherulites ranging in diameter from 5 to 20 µm (maximum dimension), with the majority of spherulites packed together edge to edge (arrow indicating longitudinal direction of fibre). This was in accordance with observations made using environmental scanning electron microscopy on the same fibre sample. the lines running along the length direction in Fig. 1 are probably artefacts caused by the sudden and relatively large change in vertical deflection experienced by the cantilever. Fig. 2(a) shows an image of the same gravity spun fibre at a higher magnification. Some of the spherulite boundaries have grown into neighbouring boundaries, whereas other spherulites have had more space to grow, resulting in defined spherulite centres. Fig. 2(b) is a line profile of the central spherulite in Fig. 2(a), demonstrating how the centre

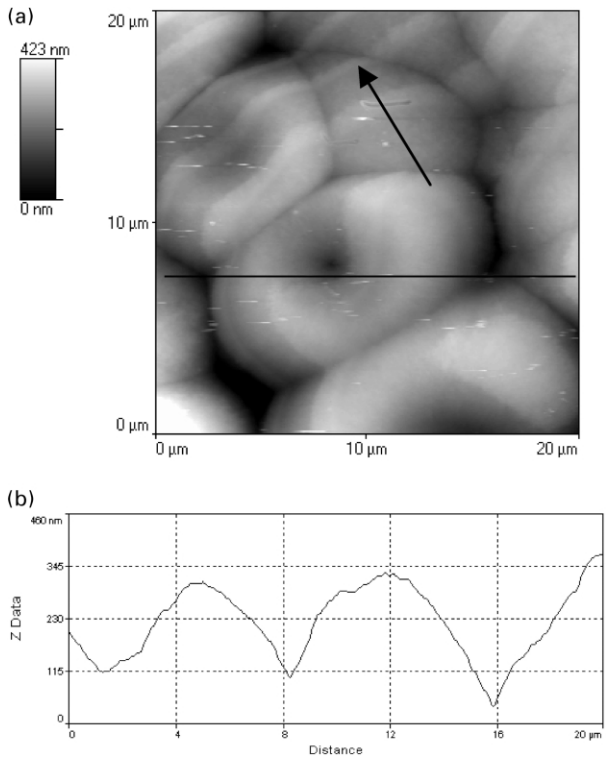

Fig. 2. (a) Topography of gravity spun PP scanned by AFM in contact mode at higher magnification relative to Fig. 1. (b) Surface profile of gravity spun PP measured along horizontal line in (a).

is situated well below the edges of the spherulites (valley type). Fig. 3(a) is an AFM scan of a single valley type spherulite from the gravity spun filament, clearly showing the centre and the edge to edge boundaries of neighbouring spherulites. The granular or nodular subspherulitic structure starts to appear and can be further resolved by LFM choosing a smaller scan area (Fig. 3(b)), (centre of spherulite inside the square frame). The valley type spherulite centre shown in Fig. 3(a) was the most common type of spherulite centre found in the cases of gravity spun and as-spun filaments. Fig. 4(a) shows a different type of spherulite centre, where the actual centre is raised relative to most of the central regions of the spherulite, as seen from Fig. 4(b) (hill type). The subspherulitic structure cannot be deduced clearly from this image, but is clearly different from the nodular valley type spherulite substructure.

3.2. As-spun 100 m min^{-1}

As can be seen in Fig. 5, there were relatively small changes in surface morphology for the as-spun filament produced at a winding speed of 100 m min^{-1} when compared to the gravity spun filament. The same characteristic valley type spherulites were found. The biggest change visible was the size of spherulites, now with maximum dimension in the region of 3–10 µm. The spherulites also seem to be slightly more orientated towards the stretch direction of the fibre compared to those of the

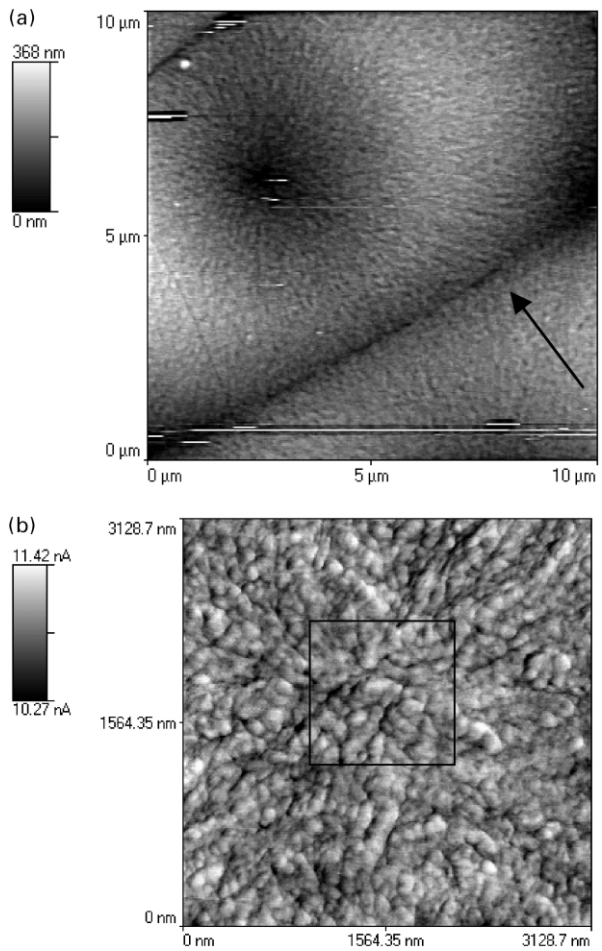

Fig. 3. (a) Topography of single valley type spherulite from gravity spun PP scanned by AFM in contact mode. (b) LFM scan of subspherulitic structure (valley type) from gravity spun PP.

gravity spun sample. At higher magnification, the subspherulitic structure can be clearly seen with both AFM (Fig. 6(a)) and LFM scans (Fig. 6(b) and (c)). The nodules are radiating out from the centre of the spherulites and are still closely packed together as shown in Fig. 6(c), albeit in what appears to be a slightly different network to the one found in spherulites from the gravity spun PP (Fig. 3(b)). The usefulness of simultaneous LFM scans to enhance surface details is clearly demonstrated in these images (Fig. 6(b) and (c)).

3.3. As-spun 200 m min^{-1}

At a winding speed of 200 m min^{-1}, the spherulites are still present but the increased stretching of the filament starts to influence their orientation and size (Fig. 7). The maximum dimension is in the region of 2–5 µm with clear signs of elongation towards the longitudinal direction of the fibre. It can also be seen that the spherulites are less packed together than in the gravity spun and as-spun 100 m min^{-1} variants.

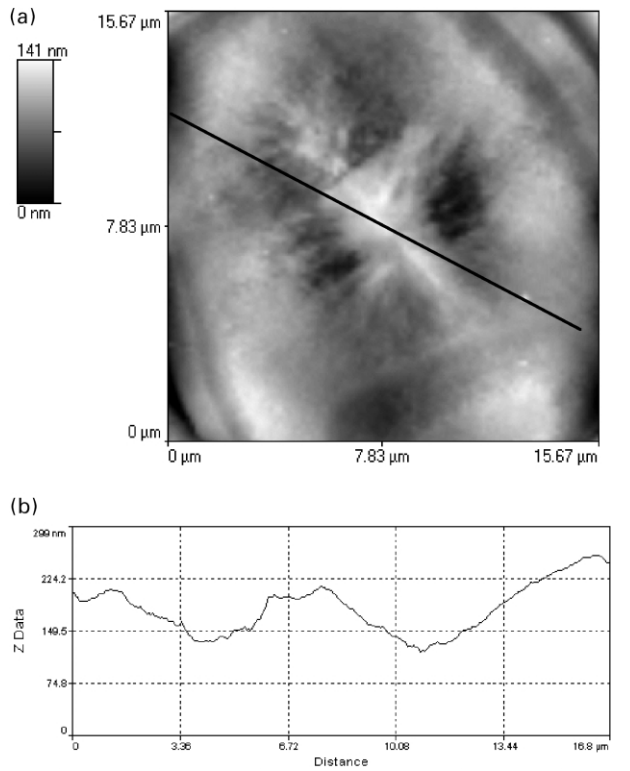

Fig. 4. (a) Topography of single hill type spherulite from gravity spun PP scanned by AFM in contact mode. (b) Surface profile of hill type spherulite measured along diagonal line in (a).

3.4. As-spun 300 m min^{-1}

The trend observed for the as-spun 200 m min^{-1} variant is further enhanced for the as-spun 300 m min^{-1} variant. The spherulites are clearly deforming as the filament experiences more stretch (Fig. 8). The morphology is, however, still more spherulitic than fibrillar in character.

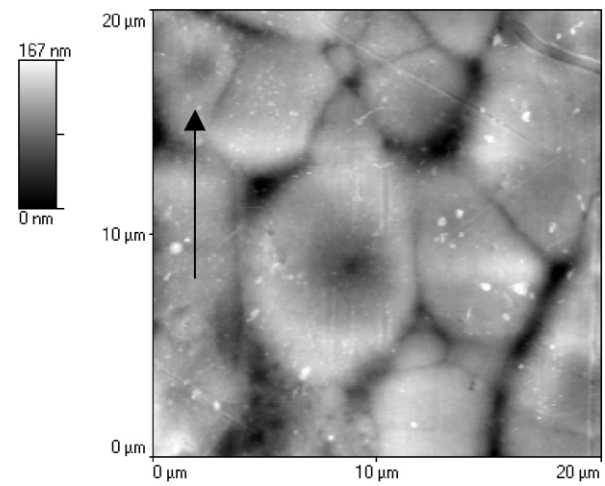

Fig. 5. Topography of as-spun 100 m min^{-1} PP scanned by AFM in contact mode.

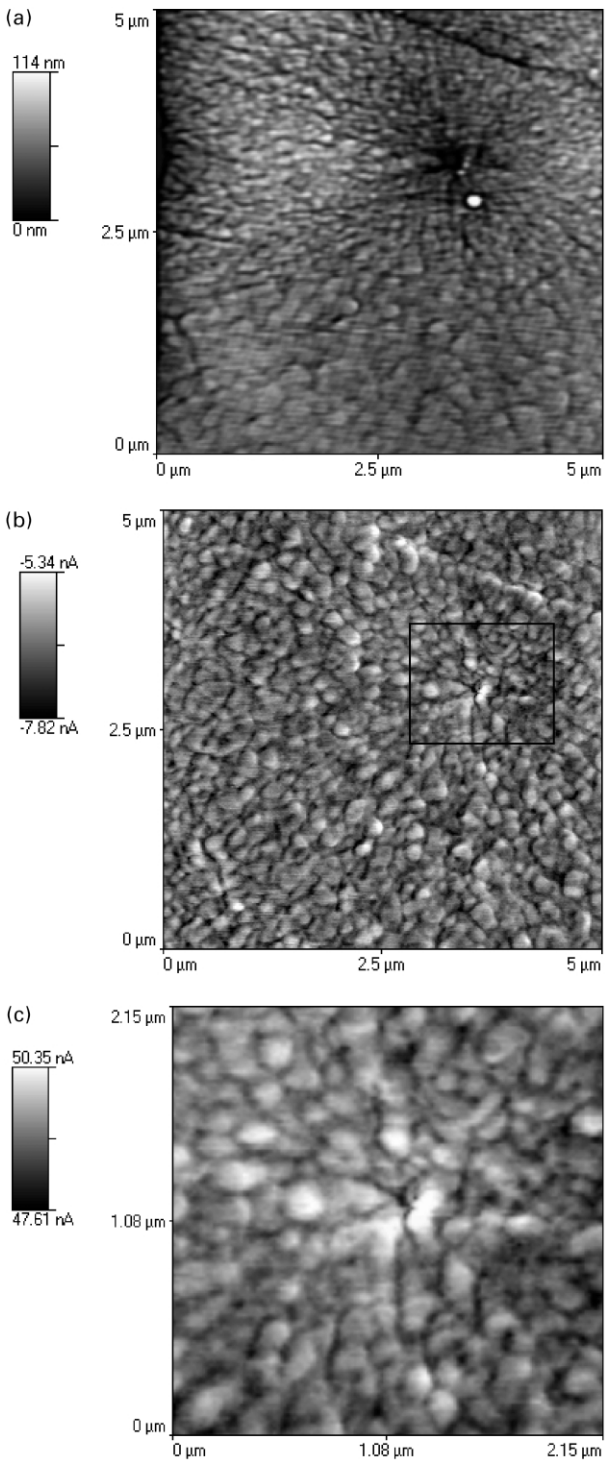

Fig. 6. (a) Topography of single valley type spherulite from as-spun 100 m min^{-1} PP scanned by AFM in contact mode. (b) LFM scan corresponding to (a). (c) LFM scan of spherulite centre (indicated by square in (b)).

3.5. As-spun 400 m min^{-1}

As seen from the as-spun 400 m min^{-1} images (Fig. 9(a) and (b)), the spherulites are now almost completely deformed and areas with a more fibrillar type structure

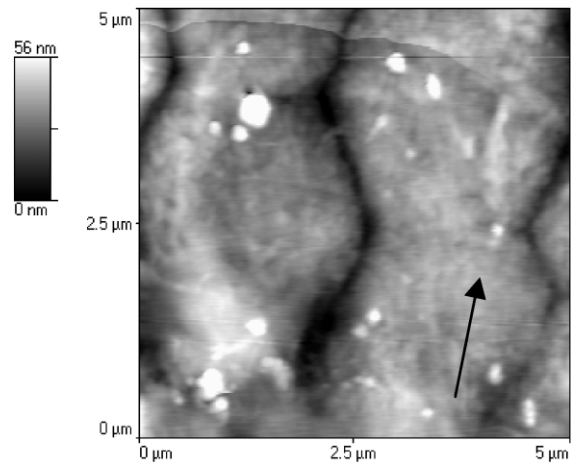

Fig. 7. Topography of as-spun 200 m min^{-1} PP scanned by AFM in contact mode.

appear as seen from the LFM image in Fig. 9(b). At higher magnification, the presence of shish-kebab type morphology can be seen (Fig. 9(c)).

3.6. Cold drawn

The cold drawn (23 °C) filament was drawn to a ratio of 4.0 and a diameter of 22 µm. A fibrillar type surface morphology can clearly be seen from Fig. 10(a). It can be observed from Fig. 10(b) that these nanofibrils have a diameter in the region of 80–100 nm and that they appear to be between 150 and 200 nm in length. A shish-kebab type structure is present, but with both the epitaxially grown crystals and the fibrillar crystals starting to stretch more with the length direction of the fibre compared to the structure seen for the as-spun 400 m min^{-1} (Fig. 9(c)).

3.7. 1-Stage hot drawn

Like the cold drawn variant, the 1-stage hot drawn

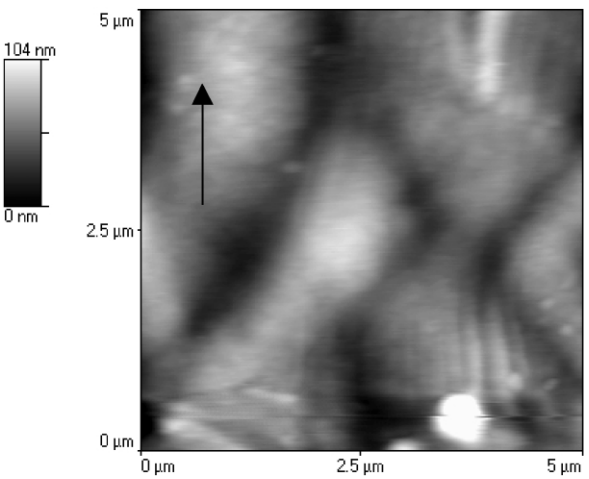

Fig. 8. Topography of as-spun 300 m min^{-1} PP scanned by AFM in contact mode.

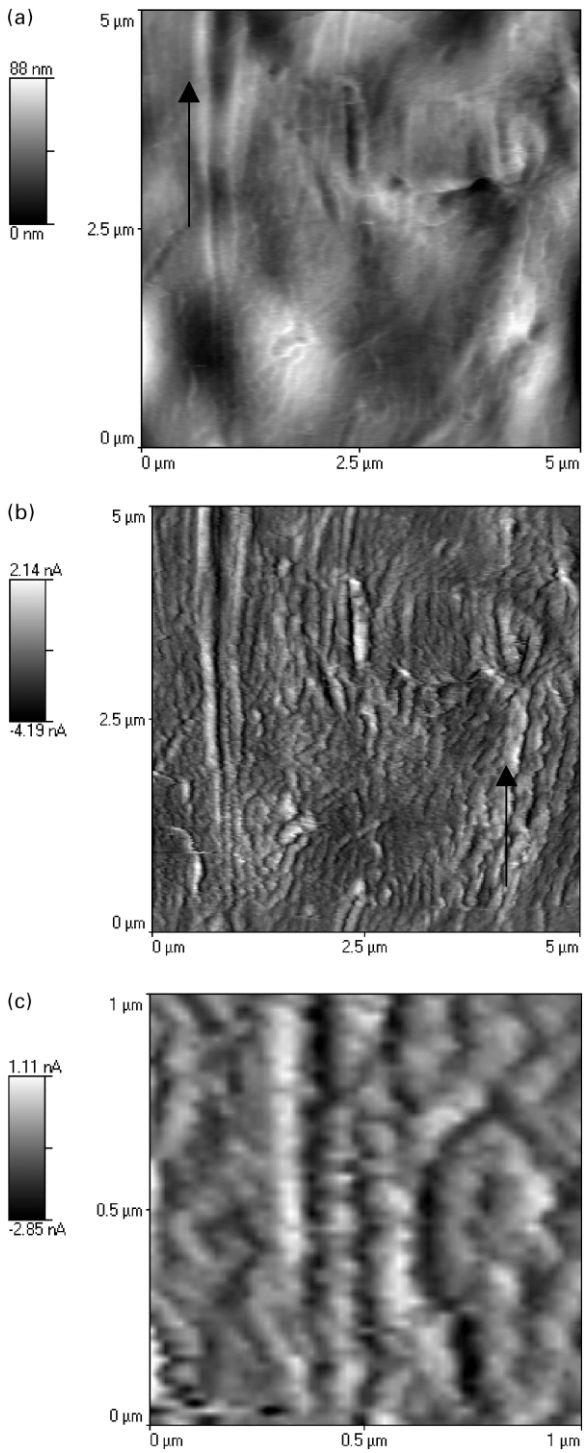

Fig. 9. (a) Topography of as-spun 400 m min^{-1} PP scanned by AFM in contact mode. (b) LFM scan corresponding to (a). (c) LFM scan of as-spun 400 m min^{-1} PP at higher magnification relative to (b).

(60 °C) filament was drawn to a ratio of 4.0. The diameter was 43 μm, significantly larger than for the cold drawn. A fibrillar and shish kebab type morphology is present (Fig. 11(a)), but with less defined nanofibrils than the cold drawn fibre (Fig. 11(b)). The AFM scan in Fig. 11(c) and the corresponding line scan (Fig. 11(d)) show that microfibrils

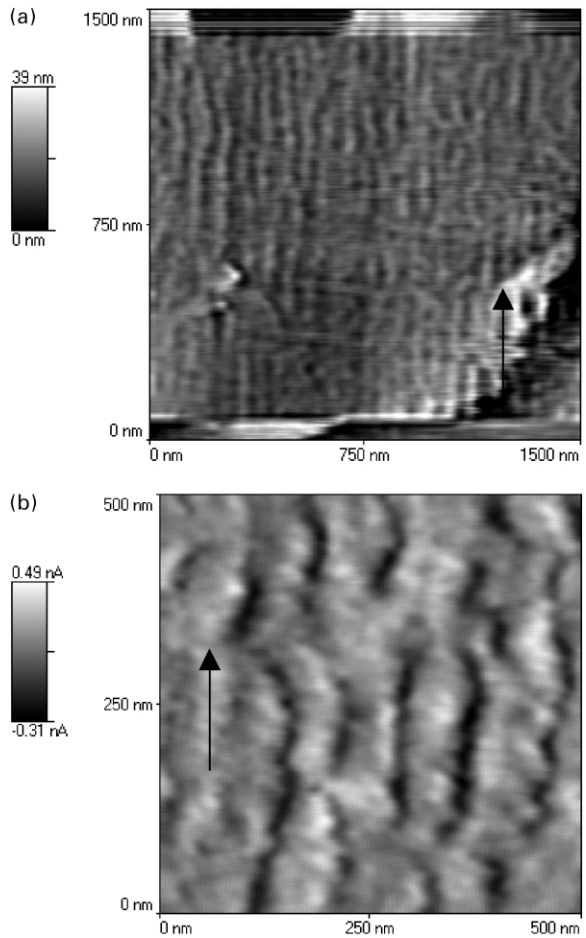

Fig. 10. (a) Topography of cold drawn PP scanned by AFM in contact mode. (b) LFM scan of cold drawn PP at higher magnification relative to (a).

with a diameter between 1 and 3 μm are present in addition to the aforementioned nanofibrils (Fig. 11(a) and (b)).

3.8. 2-Stage hot drawn

As described in Section 2, the 2-stage hot drawn filament was first drawn as the 1-stage hot-drawn variant at 60 °C to a ratio of 4.0, before second stage drawing at 150 °C to a total ratio of 11.5. The filament had a diameter of 31 μm. The AFM image in Fig. 12(a) shows a significant change in the nanofibrillar characteristics for 2-stage hot drawn relative to that of the cold drawn and 1-stage hot drawn fibres. The fibrils seem flattened and more continuous. The diameter of the nanofibrils is 80–100 nm, similar to what was found for the other two drawn variants. Fig. 12(b) shows how smooth the nanofibrils are at this draw ratio and temperature compared to the results found at lower draw ratio and temperature.

3.9. WAXS data

The WAXS diffractometer trace for the gravity spun

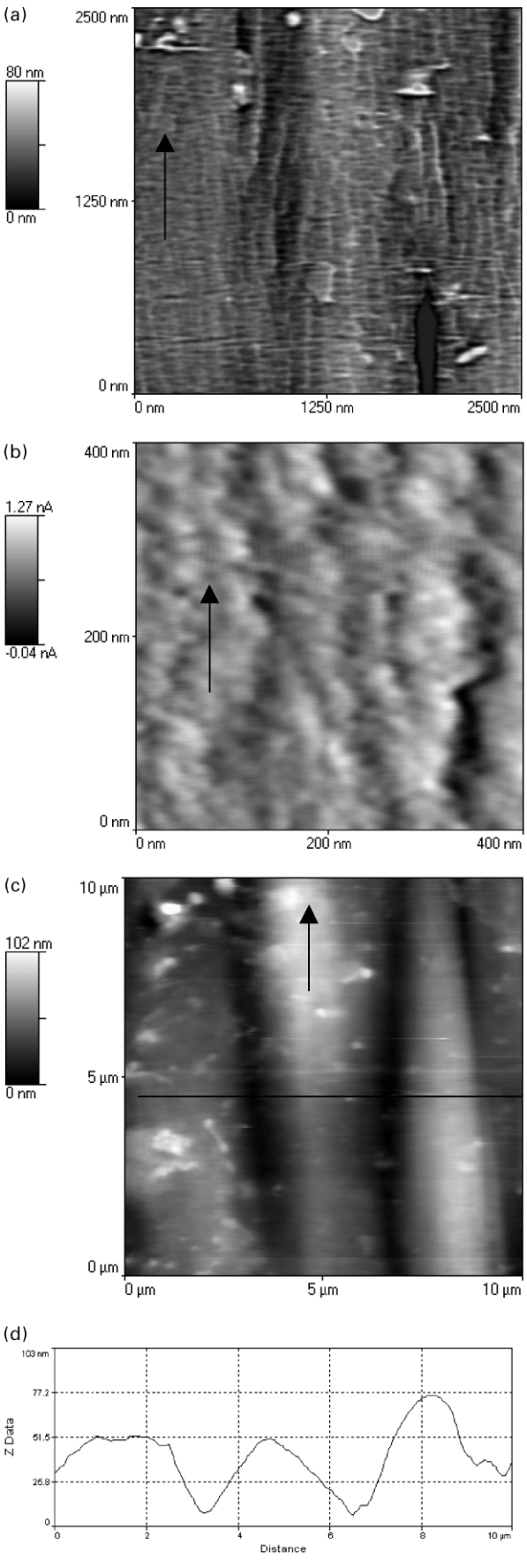

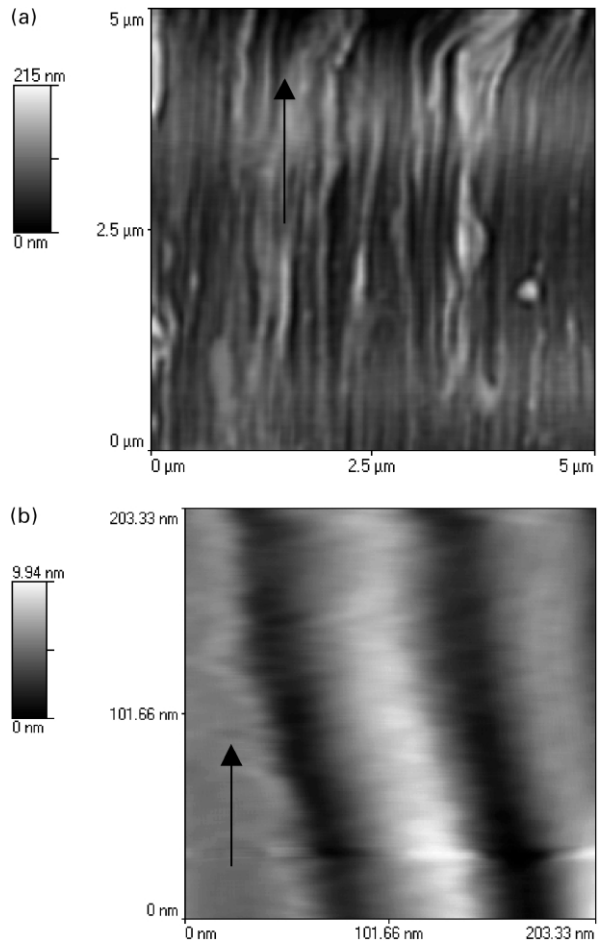

Fig. 12. (a) Topography of 2-stage hot drawn PP scanned by AFM in contact mode. (b) Topography of individual nanofibrils from 2-stage hot drawn PP scanned by AFM in contact mode.

filament (Fig. 13(a)) indicates a predominantly crystalline structure. The four distinctive peaks are of relative low intensity with a significant amount of background area reflecting the presence of amorphous regions. The peaks are present at approximately 14.5, 17, 19, and 22°.

Fig. 13(b) shows the X-ray diffraction for the various PP as-spun filaments. The as-spun 100 m min^{-1} (trace 1) has the highest intensity diffraction trace of the four as-spun fibres, with intensity decreasing as winding speed increases. The two most distinctive peaks are at approximately 15 and 22° for the as-spun samples. The as-spun 100–300 m min^{-1} samples (traces 1–3, respectively) also have peaks at 17 and 19°, but of very weak intensity compared to the gravity spun fibre. These as-spun variants have a diffraction trace indicating a transitional structure (a change from crystalline to paracrystalline (smectic) or vice versa). The as-spun

Fig. 11. (a) Topography of 1-stage hot drawn PP scanned by AFM in contact mode. (b) LFM scan of 1-stage hot drawn PP at higher magnification relative to (a). (c) Topography of 1-stage hot drawn PP at lower magnification relative to (a). (d) Surface profile of 1-stage hot drawn PP measured along horizontal line in (c).

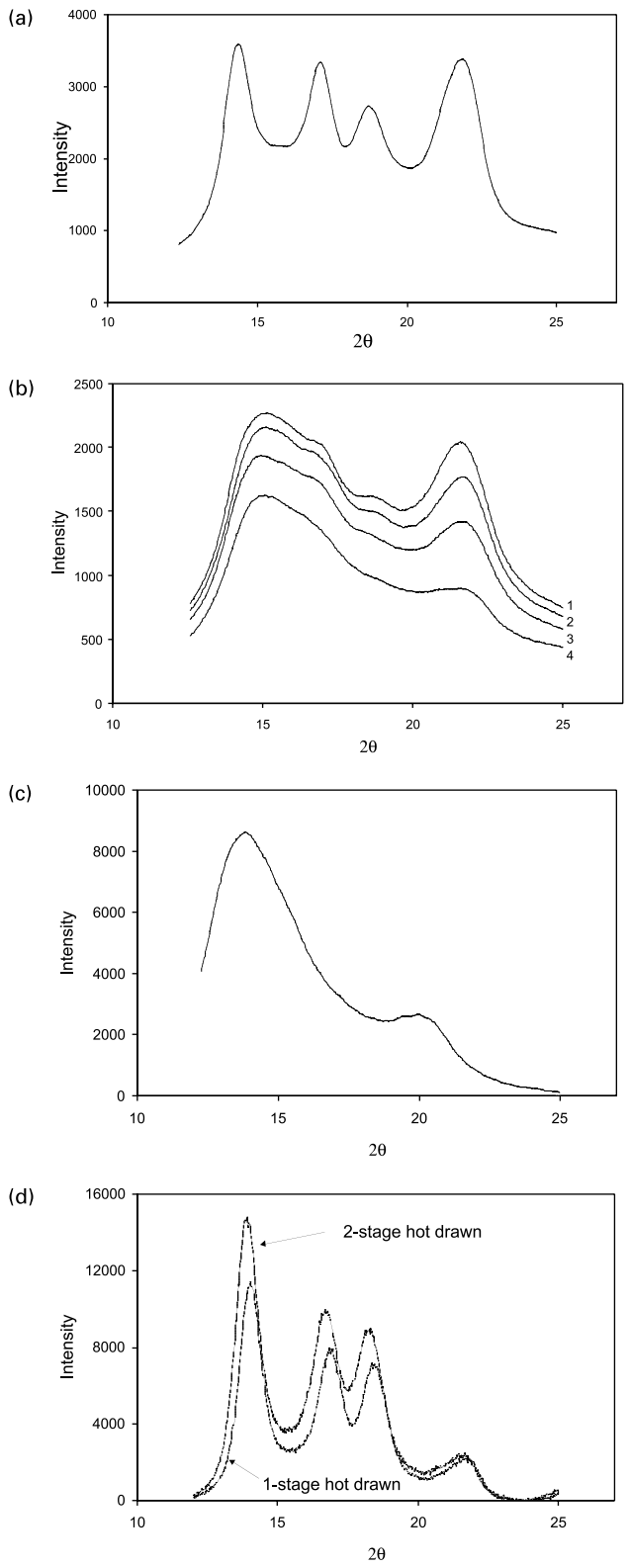

Fig. 13. (a) WAXS diffraction pattern of gravity spun PP. (b) WAXS diffraction pattern of the various as-spun PP filaments. (1) 100 m min^{-1}, (2) 200 m min^{-1}, (3) 300 m min^{-1}, (4) 400 m min^{-1}. (c) WAXS diffraction pattern of cold drawn PP. (d) WAXS diffraction pattern of hot drawn PP.

400 m min^{-1} (trace 4 in Fig. 13(b)) only has peaks at 15 and 22° with a diffraction trace typical for a paracrystalline structure [29].

The diffraction trace for the drawn filaments can be seen in Fig. 13(c). The drawn variants were produced from the as-spun 200 m min^{-1}. The cold drawn PP fibre has peaks at 14° and 20° showing a paracrystalline character. Compared to the as-spun 400 m min^{-1} filament, which is also paracrystalline, the cold drawn filament has its diffraction peaks closer together (6° cf. 7° for the as-spun). The peaks are also more narrow and of higher intensity in the case of the cold drawn fibre and thus less amorphous regions are indicated compared to the as-spun 400 m min^{-1} variant.

Both hot drawn variants contain highly crystalline regions as seen from Fig. 13(d). The 2-stage hot drawn filament shows overall a higher intensity diffraction trace relative to the 1-stage hot drawn. The peak at 22° has a much lower intensity for the drawn filaments when compared to the gravity spun and as-spun filaments.

4. Discussion

4.1. SPM methodology

There currently exist a range of SPM techniques that can be applied to the analysis of polymeric materials. For topography imaging, AFM in contact-, intermittent contact-(tapping) or non-contact modes are possible methods and there have been several publications debating whether contact mode or intermittent contact mode is preferable for relatively soft materials such as polymers. Magonov and Reneker found that damage by the tip to the sample surface is likely at high tip-to-sample forces in contact mode scanning of polymeric materials, especially the presence of lateral forces [30]. Wawkuschewski et al. compared contact mode and intermittent contact mode images of polyethylene nanofibrils (3 nm in diameter) and found less damage to these fibrils in intermittent contact mode [31]. Spatz et al. developed a model to monitor the actual tip-to-sample forces [32] and found that even with intermittent contact mode there is a risk of surface damage if too high a frequency is employed.

The difference in results between research groups studying Kevlar fibres was partly attributed to the difference in applied methodology [15,17]. It was suggested that the use of contact mode had mechanically deformed the top surface of the fibre causing the pleated periodical structure to twist and overlap. These structural features were reported to have dimensions in the region of 50 nm. The nanofibrils observed in the work reported in this paper were 80–100 nm in diameter with no apparent damage caused by scanning in contact mode using a low spring constant cantilever and scan force set point of 35 nA or less. This was verified by scanning the same area several times in LFM mode, with subsequent imaging confirming no visible damage to the samples. Surface

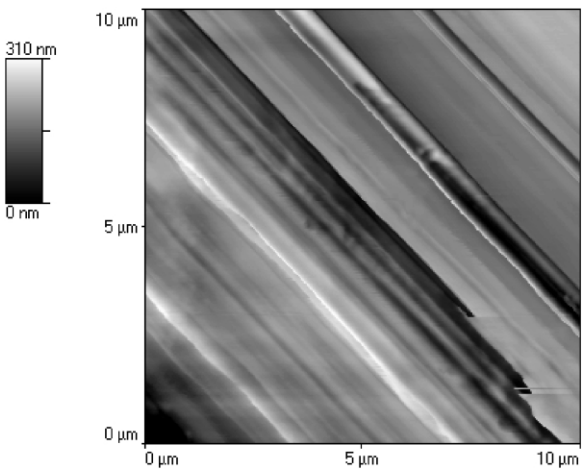

Fig. 14. Topography artefacts from AFM scan in contact mode of as-spun 100 m min^{-1} PP.

damage caused by a soft tip on fibre surface features is more likely to be a factor if the aim is to produce images on a molecular scale, since the apex of the tip will have dimensions closer to the scale of the features to be scanned.

Contact mode is a requirement if LFM is to be applied in conjunction with AFM. In this study, LFM has been shown to be a powerful technique that can reveal enhanced surface detail due to the increased lateral force experienced by the tip at edges of topographic features. As such, contact mode is a valid choice of technique and indeed the high resolution images of spherulitic and subspherulitic structure obtained with LFM verifies that this is an effective choice. It is clear from the LFM images that the features seen are complementary to those observed in the AFM images, but with a substantially higher definition of structural detail. This supports the findings by Nie et al. on PP films [27].

It is important to stress that LFM data should only be interpreted with regard to topographic detail when compared to the AFM image obtained simultaneously. Due to the rounded nature of fibres, the cantilever, with a maximum theoretical vertical travel of 8 µm, is incapable of scanning more than a limited part of the available fibre surface. Fibres can, in addition, be quite corrugated causing localised artefacts in an image. Fig. 1 clearly demonstrates the type of topographical artefact that is likely to appear when scanning a relative large proportion of a curved surface. These artefacts were found to be even more pronounced in LFM. LFM was therefore found to be most informative at higher magnification where corrugation and curvature became less of an issue. It was also found that if the cantilever tip is not positioned exactly on top of the fibre curve there is a high chance that the image obtained will not contain any real surface features from the sample, as demonstrated in Fig. 14 (as-spun PP).

4.2. PP fibre morphology—gravity spun and as-spun

In the gravity spun and as-spun filaments with a low degree of drawing, the morphology was dominated by spherulitic structures. This corresponds to observations made by De Rovere et al. on gravity spun PP filaments and Hautojarvi et al. on as-spun PP filaments [9–11]. The subspherulitic structure is more dense and regular compared to the regions between spherulites, thus forming clearly defined boundaries. The valley type spherulites had a nodular substructure, also consistent with previous observations on i-PP [9–11]. This type of substructure has been reported for α-type spherulites [33]. The α-spherulite consists of two types of lamellae; a radial (mother) and a tangential (daughter) type [34]. The nodular rather than lamellar appearance is due to the large number of daughter lamellae, with nodules corresponding to cross-hatched branching between mother and daughter lamellae [33]. The α-spherulites are reported to have a monoclinic structure [35] and will give rise to characteristic peaks in WAXS traces, which are readily distinguished from those given by the β and γ-type [35,36]. The WAXS result for the gravity spun filament clearly indicates that the α-form is dominant, confirming the SPM results where only one 'mountain' type spherulite was observed (Fig. 4(a)) and all other spherulites seen were of the α-form (valley type). The mountain type spherulite is tentatively suggested to be the β-type with radial lamellae. These lamellae are less dense than those found in the α-type (valley) spherulites. Both structural forms can be found within a common temperature range of crystallisation [37], but the monoclinic α-form is the thermodynamically more stable of the two crystalline forms [38]. The third form is the γ-type, which has been shown to require higher pressure or lower molecular weight PP than conditions used for this work to be formed [39–41].

A paracrystalline or 'smectic' structure may also be assumed by PP. This is suggested to be a combination of glass and a mesomorphic phase with helical conformation [42]. The paracrystalline form is less ordered, but not amorphous [42]. It is easily obtained by rapid cooling of the polymer melt in a liquid bath [43], but has also been produced under air-cooling conditions [44]. The crystallisation rate and degree of crystallinity of as-spun filaments depend upon a number of factors relating to material properties and processing conditions, as demonstrated by Yang et al. [25]. The as-spun filaments used in this work were made from the same raw polymer, the only variable being winding speed. Previous work on as-spun filaments has concluded that an increase in spin-line stress, e.g. by increasing winding speed, enhances crystallisation rate and degree of crystallinity [45]. This is in contrast to the observations made in this work, where WAXS patterns indicate that there is a significantly lower degree of crystallinity for the as-spun filaments when compared to the gravity spun filament. In fact, crystallinity is decreasing as winding speed increases from 100 to 400 m min^{-1}. The as-spun fibre produced at a winding speed of 400 m min^{-1} has a WAXS pattern similar to that previously reported for the paracrystalline form [25]. The 100–300 m min^{-1} variants are largely in the paracrystalline form with some

weak signals indicating the presence of α-form. This has been referred to as a transitional structure [25].

The SPM images indicate only minor changes in surface structure between gravity spun and as-spun 100 m min^{-1} fibres. The α-type spherulites are similar in appearance with perhaps a slightly less dense population of lamellar nodes in the as-spun variant. This is perhaps indicating that the decrease in crystallinity observed by WAXS going from gravity spun to as-spun is mainly happening in the subsurface regions. As the winding speed is increased from 100 to 400 m min^{-1} for the as-spun filaments the spherulites start to deform. At 200 m min^{-1} they become more ellipsoidal and orientated with the length direction of the fibre. At 300 m min^{-1} cavities between the deformed spherulites become more pronounced (Fig. 8). These observations are in agreement with work by Aboulfaraj et al. [46] on PP and are postulated to be due to the α-type's brittle behaviour under tensile loading. This brittleness also offers an explanation for the minor change in surface morphology between gravity spun and as-spun 100 m min^{-1} when WAXS patterns clearly indicate a significant change in degree of crystallinity. Aboulfaraj et al. [46] suggested that the interlocked structure of the α-spherulites was the main contributor towards their brittleness. They found that the α-structure deformed less than the global deformation and that plastic slide was very difficult in this phase relative to the β-type structure [46]. Therefore, if the core of the monofilament consists of, for example, α-structure with more defects, or more amorphous regions than the surface, it may deform to a higher extent and so overall decrease the degree of crystallinity of the fibre. Differences in orientation between skin and core for PP filaments have previously been observed [47] and should also be considered. Cross-sectional analysis is in progress and may provide some answers to these suggestions.

An additional explanation for the higher degree of crystallinity of the gravity spun compared to the as-spun variants is perhaps the difference in cooling rates experienced by these filaments. It has been reported that an increase in cooling rate leads to an increase in defects in crystallites [48]. The core of the gravity spun fibre will have a slower cooling rate than the core of the as-spun variants due to its significantly larger diameter (three times larger compared to the as-spun 400 m min^{-1}) and therefore a smaller proportion of crystallites with defects. This trend continues throughout the as-spun series of filaments, with the as-spun 400 m min^{-1} being the least crystalline.

At a winding speed of 400 m min^{-1} the surface morphology of the as-spun filament consists of heavily deformed spherulites, shish-kebab structures and the initial formation of fibrils (Fig. 9(a)–(c)). The WAXS pattern shows that the filament is overall paracrystalline. Shish-kebab structures were recently observed on melt spun and compact spun PP by SPM [9,10]. The molecular arrangement in a shish-kebab structure is not ideal for most end products, because of the non-stress carrying epitaxially grown crystals [49].

4.3. PP morphology—drawn filaments

The WAXS pattern of the cold drawn filament indicates that it is in a paracrystalline form. This was also found to be the case for the as-spun 400 m min^{-1}, but with less intensity than the cold drawn. Similar comparison is usefully made between SPM images for the same group of filaments. It can be seen that there are no signs of spherulites on the surface of the cold drawn fibre and that nanofibrils are present (Fig. 10(a)). However, these are not continuous and are possibly a late stage shish-kebab type structure where the epitaxially grown crystals observed for the as-spun 400 m min^{-1} fibre (Fig. 10(b)) have been stretched and oriented parallel to the draw direction in the case of the cold drawn fibre.

When the WAXS pattern for the cold dawn filament is compared to that of the 1-stage hot drawn (60 °C), it can be seen that the increased temperature increases the degree of crystallinity. This increase is not reflected in the overall orientation on the fibre surface. The 1-stage hot drawn has a less defined fibrillar surface morphology relative to the cold drawn variant, which is clearly seen when compared at higher magnification (Figs. 10(b) and 11(b)). This contrasts slightly to findings by Hautojarvi et al. where no difference in surface morphology was observed between cold drawn and 1-stage hot drawn (90 °C) [9]. However, there are differences in the raw polymer, processing parameters, fibre diameter and a 30 °C difference in temperature, which could account for the anomalies. A possible explanation for the differences observed in this work lies in the actual drawing mechanisms that take place. In a cold drawn PP filament the drawing process happens through necking. Nadella et al. [45] found that cold drawing transforms a monoclinic as-spun filament into a more oriented but disordered structure with decreased crystallite size, increased lattice strain and defects similar to the paracrystalline form. This is confirmed by the orientated surface morphology and paracrystalline WAXS pattern found in this work.

It should be pointed out that the paracrystalline diffraction pattern observed for the cold drawn fibre differs with regards to shape and the 2θ values at which the peaks appear when compared to the WAXS patterns determined for as-spun 200–400 m min^{-1} filaments. Fig. 13(b) shows how the WAXS pattern gradually transforms from a weak monoclinic α-type form (transitional) for the as-spun 100 m min^{-1} to a pure paracrystalline form for the as-spun 400 m min^{-1}. The two peaks observed for the paracrystalline form are at approximately 15 and 22°. The differences between each of the 2θ-values in the WAXS pattern (14 vs. 15° and 20 vs. 22°) for the cold drawn and as-spun 400 m min^{-1}, whilst small, appear significant. Moreover, the two peaks for the cold drawn fibre are separated by 6°, compared to the 7° separation observed for the as-spun 400 m min^{-1} fibre. Thus the overall shape of the WAXS

pattern appears different between the cold drawn and as-spun variant.

It can be observed that the positions of the diffraction peaks for the cold drawn fibre closely match those for two of the peaks previously observed for the PP γ-form [36]. Further experiments are required to confirm the possible presence of a paracrystalline γ-form. This is of interest since oriented fibres of the γ-form have yet to be produced, and a paracrystalline γ-form might be considered as a first step in that direction.

The 2-stage hot drawn (60 °C/150 °C) filament has both a high degree of crystallinity and a highly oriented surface morphology with continuous nanofibrils. The 1-stage hot drawn filament has almost the same degree of crystallinity, but, as mentioned above, not such a well defined fibrillar surface structure as the cold drawn and the 2-stage hot drawn filaments in particular. The difference between the two hot-drawn filaments is in accordance with observations made by Samuels [50] where he showed that below the crystal mobility temperature (CMT), of 110 °C the crystal lamellae are resistant to orientation. Deformation below this temperature is controlled mainly by non-crystalline areas. The increased crystal mobility above the CMT allows the lamellae to slip and rotate, enabling them to orientate their chain axes along the fibre axis and thus complete the transformation from spherulitic structure to fibrillar structure.

5. Conclusions

From this experimental study the following conclusions can be drawn:

1. SPM, specifically AFM and LFM provides valuable surface information at high resolution to help define the structure of PP polymer fibres. No deformation of the fibre by the cantilever tip occurred using contact mode scanning.
2. A spherulitic structure dominates the fibre surface in gravity spun and as-spun fibres of low draw-down ratio. SPM imaging reveals, as winding speed increases, that there is a gradual deformation of the spherulites into a shish-kebab type structure. For drawn filaments the surface structure is predominantly fibrillar in character.
3. WAXS results, in conjunction with SPM, serve to elucidate the contrasting features of surface and bulk crystal structure.
4. The SPM and WAXS results in this work highlight the importance of studying both internal and external morphology at all stages of production when optimising production parameters.

Acknowledgements

The authors wish to thank Heriot-Watt University for financial support; Marian K. Millar and Stewart Wallace for assistance and technical support in the use of SPM, WAXS, and extrusion facilities, respectively; Gary Loveridge at Becton Dickinson for measurements of MFI data of the raw materials. The authors also wish to thank Borealis for the provision of raw PP material.

References

[1] Pereira RS. Biochem Pharmacol 2001;62:975.
[2] Gwo S. J Phys Chem Solids 2001;62:1673.
[3] Magonov S, Whangbo M-H. Surface analysis with STM and AFM. Weinheim: Wiley-VCH; 1996.
[4] Titcombe LA, Huson MG, Turner PS. Micron 1997;28:69.
[5] Jovancic PM, Jocic DM. Tekstilna Ind 1998;46:5.
[6] Parbhu AN, Bryson WG, Lal R. Biochemistry 1999;38:11755.
[7] Crossley JAA, Gibson CT, Mapledoram LD, Huson MG, Myhra S, Pham DK, Sofield CJ, Turner PS, Watson GS. Micron 2000;31:659.
[8] Leijala A, Hautojarvi J. Textile Res J 1998;68:193.
[9] Hautojarvi J, Leijala A. J Appl Polym Sci 1999;74:1242.
[10] Hautojarvi J, Niemi H. Textile Res J 2000;70:820.
[11] De Rovere A, Shambaugh RL, O'Rear EA. J Appl Polym Sci 2000;77:1921.
[12] Magonov SN, Qvarnstrom K, Elings V, Cantow HJ. Polym Bull 1991;25:689.
[13] Magonov SN, Sheiko SS, Deblieck RAC, Moller M. Macromolecules 1993;26:1380.
[14] Dilsiz N, Wightman JP. Carbon 1999;37:1105.
[15] Li SFY, McGhie AJ, Tang SL. Polymer 1993;34:4573.
[16] Rebouillat S, Donnet J-B, Tong Kuan W. Polymer 1997;38:2245.
[17] Rebouillat S, Peng JCM, Donnet J-B. Polymer 1999;40:7341.
[18] Graham JF, McCague C, Warren OL, Norton PR. Polymer 2000;41:4761.
[19] Klein N, Marom G, Wachtel E. Polymer 1996;37:5493.
[20] Vancso GJ, Liu G, KargerKocsis J, Varga J. Colloid Polym Sci 1997;275:181.
[21] Wu CM, Chen M, Karger-Kocsis J. Polym Bull 1998;41:239.
[22] Pastore CM. Surface characteristics of fibres and textiles. New York: Marcel Dekker; 2000.
[23] Byrne C, Anand SC. In Horrocks AR, editor. Handbook of technical textiles, Cambridge, UK: The Textiles Institute, Woodhead Publishing Ltd., 2000.
[24] Peckstadt J-P. Polypropylene in textiles. Huddersfield: University of Huddersfield; 2000. p. 147.
[25] Yang RD, Mather RR, Fotheringham AF. Int Polym Process 1999;14:60.
[26] IUAPAC. Compendium of Chemical Terminology; 1997.
[27] Nie HY, Walzak MJ, McIntyre NS, El-Sherik AM. Appl Surf Sci 1999;145:633.
[28] Andreassen E, Myhre OJ, Oldervoll F, Hinrichsen EL, Grostad K, Braathen MD. J Appl Polym Sci 1995;58:1619.
[29] Cohen Y, Saraf RF. Polymer 2001;42:5865.
[30] Magonov SN, Reneker DH. Annu Rev Mater Sci 1997;27:175.
[31] Wawkuschewski A, Cramer K, Cantow HJ, Magonov SN. Ultramicroscopy 1995;58:185.
[32] Spatz JP, Sheiko S, Moller M, Winkler RG, Reineker P, Marti O. Nanotechnology 1995;6:40.
[33] Norton DR, Keller A. Polymer 1985;26:704.
[34] Castelein G, Coulon G, Aboulfaraj M, Gsell C, Lepleux E. Journal De Physique Iii 1995;5:547.
[35] Natta G, Peraldo M, Corradini P. Rend Accad Naz Lincei 1959;26:14.
[36] Mezghani K, Phillips PJ. Polymer 1997;38:5725.
[37] Padden FJ, Keith HD. J Appl Phys 1959;30:1479.
[38] Lotz B, Wittmann JC. Polymer 1996;37:4979.
[39] Addink E, Beintema J. Polymer 1961;2:185.

[40] Kardos JL, Christiansen JL, Baer E. J Polym Sci, Part A-2 1966;4:777.
[41] Pae KD, Morrow DR, Sauer JA. Nature 1966;211:514.
[42] Corradini P, Petraccone V, De Rosa C, Guerra G. Macromolecules 1986;19:2699.
[43] Natta G, Corradini P. Nuovo Cimento 1960;15(Suppl.):40.
[44] Wang IC, Dobb MG, Tomka JG. J Textile Inst 1995;86:383.
[45] Nadella H, Henson HM, Spruiell JE, White JL. J Appl Polym Sci 1977;21:3003.
[46] Aboulfaraj M, Gsell C, Ulrich B, Dahoun A. Polymer 1995;36:731.
[47] Fung PYF, Orlando E, Carr SH. Polym Engng Sci 1973;13:295.
[48] Akay M. Second International Conference on Polypropylene Fibres and Textiles, York, UK, 1979.
[49] Porter RS, Kanamoto T. In Seymour RB, editor. Manmade Fibres: Their origin and development, London/New York: Elsevier Applied Science, 1998, p. 295.
[50] Samuels RJ. J Polym Sci, Part A 1968;6:2021.